HHS Public Access

Author manuscript

Nat Neurosci. Author manuscript; available in PMC 2013 January 01.

Published in final edited form as:

Nat Neurosci. ; 15(7): 970–978. doi:10.1038/nn.3133.

Structure and functional interaction of the extracellular domain of human $GABA_B$ receptor GBR2

Yong Geng[1], **Dazhi Xiong**[1], **Lidia Mosyak**[1], **David L. Malito**[2], **Julie Kniazeff**[3,4,5], **Yan Chen**[1], **Svetlana Burmakina**[1], **Matthias Quick**[6], **Martin Bush**[1], **Jonathan A. Javitch**[1,6], **Jean-Philippe Pin**[3,4,5], and **Qing R. Fan**[1,7]

[1]Department of Pharmacology, Columbia University Medical Center, 630 West 168th Street, New York, NY 10032, USA

[2]Department of Neuroscience, Columbia University Medical Center, 630 West 168th Street, New York, NY 10032, USA

[3]CNRS UMR 5203, Montpellier, France

[4]INSERM U661, Montpellier, France

[5]Université Montpellier 1, 2, Institut de Génomique Fonctionnelle, 141 rue de la Cardonille, F-34094 Montpellier Cedex 05, France

[6]Department of Psychiatry, Columbia University Medical Center, 630 West 168th Street, New York, NY 10032, USA

[7]Department of Pathology & Cell Biology, Columbia University Medical Center, 630 West 168th Street, New York, NY 10032, USA

Abstract

Inhibitory neurotransmission is mediated primarily by GABA. Metabotropic $GABA_B$ receptor is a G protein coupled receptor central to mammalian brain function. Malfunction of $GABA_B$ receptor has been implicated in a number of neurological disorders. $GABA_B$ receptor functions as a heterodimeric assembly of GBR1 and GBR2 subunits, where GBR1 is responsible for ligand-binding and GBR2 is responsible for G protein coupling. Here we demonstrate that the GBR2 ectodomain directly interacts with the GBR1 ectodomain to increase agonist affinity by selectively stabilizing the agonist-bound conformation of GBR1. We present the crystal structure of the

Correspondence should be addressed to Q.R.F. (qf13@columbia.edu).

ACCESSION NUMBERS

Atomic coordinates and diffraction data are deposited in the RCSB Protein Data Bank with accession codes 4F11 and 4F12.

SUPPLEMENTAL INFORMATION

Supplemental Information includes five figures and five tables.

AUTHOR CONTRIBUTIONS

Q.R.F. conceived the study, designed the experiments and wrote the paper; Q.R.F., Y.G. D.X., L.M., D.L.M., Y.C., S.B., M.B. performed experiments and analyzed data; J.K. and J.P.P. designed and carried out studies of glycosylation mutants; M.Q. and J.J. supervised SPA experiments.

COMPETING INTERESTS STATEMENT

The authors declare no competing financial interests.

GBR2 ectodomain, which reveals a polar heterodimeric interface. We also identify specific heterodimer contacts from both subunits, and GBR1 residues involved in ligand recognition. Lastly, our structural and functional data indicate that the GBR2 ectodomain adopts a constitutively open conformation, suggesting a structural asymmetry in the active state of $GABA_B$ receptor that is unique to the GABAergic system.

INTRODUCTION

The function of brain circuitry involves both excitatory and inhibitory signals. Inhibitory signals are mediated primarily by the neurotransmitter γ-aminobutyric acid (GABA). GABA acts through three classes of transmembrane receptors. Ionotropic $GABA_A$ and $GABA_C$ receptors are ligand-gated ion channels that mediate fast synaptic inhibition[1]. Metabotropic $GABA_B$ receptor is a G protein-coupled receptor (GPCR) that produces slow and prolonged inhibitory activity[2,3].

$GABA_B$ receptor is distributed throughout the mammalian central nervous system. In response to GABA-binding, it regulates the activity of Ca^{2+} and K^+ channels, and inhibits the function of adenylyl cyclase through $G_{i/o}$[2,3]. Specifically, activation of $GABA_B$ receptor blocks presynaptic neurotransmitter release through the inhibition of voltage-gated Ca^{2+} channels; it also stimulates G protein-activated inwardly rectifying K^+ channels (GIRKs) to generate inhibitory postsynaptic potentials[2,3]. Disruption of $GABA_B$ receptor function has been implicated in a number of neurological diseases, including spasticity, epilepsy, pain and drug abuse[2,3]. Baclofen, a specific $GABA_B$ receptor agonist, is used clinically to treat muscle spasticity in patients with multiple sclerosis, brain and spinal cord injuries[2,3].

$GABA_B$ receptor is a member of the class C GPCR family, which includes metabotropic glutamate receptors (mGluRs), Ca^{2+}-sensing receptor (CaR), and some pheromone and taste receptors[4]. Class C receptors possess the characteristic seven-helix transmembrane (TM) domain responsible for receptor activation; however, their ligand-binding site is located within a large extracellular Venus Flytrap (VFT) module that has sequence homology to bacterial periplasmic amino acid binding proteins[4].

Most of the available structural information for class C GPCRs is from mGluRs. The crystal structure of the extracellular ligand-binding domain of rat mGluR1 has been solved both in the absence and presence of bound glutamate[5]. This domain forms a disulfide-linked homodimer[5,6]. Each protomer exists in a dynamic equilibrium between open and closed conformations, where the closed conformation is stabilized by glutamate-binding[5]. The homodimeric mGluR1 ectodomain is asymmetric when fully occupied by glutamate, such that one protomer adopts a closed conformation and the other protomer adopts an open conformation[5]. This results in partial receptor activation, however, full activation requires the closure of both protomers[7]. Glutamate-binding also induces a rearrangement of the dimer interface that shortens the distance between the C-termini of the two protomers[5]. It has been proposed that this rearrangement brings the mGluR TM domains together for receptor activation[4,5,8,9].

Unlike mGluRs and CaR, which function as disulfide-tethered homodimers, $GABA_B$ receptor functions as a heterodimeric assembly of the $GABA_BR1$ (GBR1) and $GABA_BR2$ (GBR2) subunits[10–14]. $GABA_B$ receptor was the first example of a GPCR that requires heterodimerization for function, and was recently followed by the discovery of obligatory heterodimerization in taste receptors[15]. $GABA_B$ heterodimerization masks an endoplasmic reticulum (ER) retention signal (RSRR) in GBR1, via a C-terminal coiled-coil interaction, to allow cell surface expression of both subunits[16]. Additionally, heterodimerization is required for ligand-induced G protein signaling[10–14].

Previous findings indicate that $GABA_B$ receptor subunits work in-concert, through a trans-activation mechanism, to carry out receptor function[4]. This hypothesis stems from asymmetries in both the TM domain and the ectodomain. First, the GBR2 TM domain contains the determinants for G protein signaling, as mutations in either the second or third intracellular loops of GBR2 abolish G protein activation[17–21]. GBR1 is not required for G protein coupling; nevertheless, its TM domain enhances coupling efficiency[18,20,22]. Second, studies using chimeric receptors indicate that both the GBR1 and GBR2 ectodomains are required for full agonist-induced activation of the receptor[18,22], in spite of the fact that only the GBR1 ectodomain is involved in ligand-recognition[23]. In fact, the GBR2 ectodomain does not bind GABA or any other known ligand[24]. Furthermore, there is evidence of non-covalent contacts between the GBR1 and GBR2 ectodomains[18,25,26]. The critical role of the GBR2 ectodomain may partially be attributed to the increased agonist-binding affinity of GBR2-bound GBR1[11,14,22,25,26], or to GBR2 ectodomain involvement in signal transduction across the membrane.

It is not known how the GBR2 ectodomain allosterically controls agonist-affinity or why it is critical for efficient trans-activation. Furthermore, no structural information is available for GBR2. In an effort to understand the functional role of the GBR2 ectodomain, we have determined its crystal structure and studied its interaction with the GBR1 ectodomain. These studies allow us to: (1) investigate the mechanism by which the non-ligand binding GBR2 ectodomain increases the agonist-binding affinity of GBR1, (2) suppose the open/closed conformation of GBR2 ectodomain in the activated state, and (3) provide insight into the heterodimeric ectodomain interface and the ligand-binding site.

RESULTS

Interaction of GBR1 and GBR2 ectodomains

We separately expressed and purified the extracellular domains of human GBR1b and GBR2 from baculovirus-infected insect cells. Different C-terminal truncations of GBR1b and GBR2 ectodomains were tested in order to determine the domain boundary of the VFT module in each subunit ($GBR1b_{VFT}$ and $GBR2_{VFT}$). Soluble $GBR1b_{VFT}$ forms mostly aggregates, but can be rescued by the addition of ligand during expression (Supplementary Fig. 1). Antagonist CGP54626 ($CGP54626_{ANT}$) is more effective than agonists GABA or SKF97541 ($SKF97541_{AGO}$) in stabilizing $GBR1_{VFT}$, possibly due to its higher affinity for the receptor. This is consistent with the thermal unfolding profiles obtained by differential scanning calorimetry (DSC), which show that $CGP54626_{ANT}$-bound $GBR1b_{VFT}$ ($GBR1b_{VFT}$-$CGP54626_{ANT}$) has a higher melting temperature than $SKF97541_{AGO}$-bound

$GBR1b_{VFT}$ ($GBR1b_{VFT}$-$SKF97541_{AGO}$) (Supplementary Fig. 1). Compared with $GBR1b_{VFT}$, a larger fraction of secreted $GBR2_{VFT}$ appears well folded (Supplementary Fig. 1). Both purified $GBR1b_{VFT}$ and $GBR2_{VFT}$ migrate faster under non-reducing conditions than under reducing conditions on an SDS gel, indicating the presence of intramolecular disulfide bonds (Supplementary Fig. 1). In addition, size-exclusion chromatography indicates that soluble $GBR2_{VFT}$ is a monomer, while $GBR1b_{VFT}$ appears to exist in a monomer-dimer equilibrium (Supplementary Fig. 1).

$GBR1b_{VFT}$ and $GBR2_{VFT}$ interact to form a heterodimer. First, size exclusion chromatography experiments demonstrate the formation of a complex with an estimated molecular mass of 104 kDa (Fig. 1a). The complex peak contains both $GBR1b_{VFT}$ and $GBR2_{VFT}$, as verified by N-terminal sequencing analysis. Individual $GBR1b_{VFT}$ and $GBR2_{VFT}$ are similar in size, with measured molecular masses of 54.6 kDa and 62.3 kDa, respectively; thus, the mass of the complex peak is consistent with a 1:1 stoichiometry. In addition, excess $GBR2_{VFT}$ drives complex formation, possibly because free $GBR1b_{VFT}$ is unstable in the absence of its binding partner. Second, direct binding between soluble $GBR1b_{VFT}$ and $GBR2_{VFT}$ could also be detected using native gel electrophoresis (Fig. 1b). The observation of a novel band in the mixture of $GBR1b_{VFT}$ and $GBR2_{VFT}$, along with the disappearance of the $GBR2_{VFT}$ band and $GBR1b_{VFT}$ smear, indicates the formation of a complex between the two subunits. This interaction between $GBR1b_{VFT}$ and $GBR2_{VFT}$ is not ligand-dependent (data not shown).

Recombinant $GBR1b_{VFT}$ is capable of recognizing various ligands. We investigated the ligand binding properties of $GBR1b_{VFT}$ by scintillation proximity assay (SPA)[27] using [^{3}H]-GABA (Supplementary Table 1a). We examined the inhibition of [^{3}H]-GABA-binding to $GBR1b_{VFT}$ by three different agonists, GABA, baclofen ($baclofen_{AGO}$) and $SKF97541_{AGO}$, as well as an antagonist, $CGP54626_{ANT}$ (Fig. 1c–f). We also studied the effect of $GBR2_{VFT}$ on ligand-binding affinity. In agreement with previous findings[3], the rank order of inhibition is $CGP54626_{ANT}$ > $SKF97541_{AGO}$ > GABA ≈ $baclofen_{AGO}$. In addition, the presence of $GBR2_{VFT}$ increases the binding affinity of all three agonists to $GBR1b_{VFT}$, as it lowers the half-maximal inhibitory concentration (IC_{50}) of GABA, $baclofen_{AGO}$ and $SKF97541_{AGO}$ by about 6–7 fold. The addition of $GBR2_{VFT}$ has no effect on the affinity of the antagonist, as the IC_{50} of $CGP54626_{ANT}$ remains essentially the same with or without $GBR2_{VFT}$. The ability of $GBR1b_{VFT}$ to bind ligands, and that of $GBR2_{VFT}$ to enhance agonist affinity, indicate that both recombinant $GBR1b_{VFT}$ and $GBR2_{VFT}$ were properly folded and functional. Nevertheless, the IC_{50} values obtained for all three ligands in the presence of $GBR2_{VFT}$ were more than 5-fold higher than that of native $GABA_B$ receptor[3,28] (Supplementary Table 1b), suggesting that the TM domains of GBR1b and GBR2 also play a role in regulating ligand affinity.

We measured the direct binding between $GBR1b_{VFT}$ and $GBR2_{VFT}$ by isothermal titration calorimetry (ITC) (Fig. 1g,h). $GBR1b_{VFT}$ protein was produced in the presence of either agonist $SKF97541_{AGO}$ or antagonist $CGP54626_{ANT}$. We found that the heterodimeric interaction is stronger between $GBR2_{VFT}$ and $GBR1b_{VFT}$-$SKF97541_{AGO}$, with a K_d of 24.9 nM. The affinity between $GBR2_{VFT}$ and $GBR1b_{VFT}$-$CGP54626_{ANT}$ is about four fold lower (K_d = 94.9 nM). The difference in binding affinities can be attributed to a much more

favorable entropy change (Δ*S*) for GBR1b$_{VFT}$-SKF97541$_{AGO}$ with GBR2$_{VFT}$, which may be rationalized by increased solvent release upon burial of additional surface during complex formation. The enthalpy changes (Δ*H*) are comparable for the two exothermic reactions, suggesting that hydrophobic interactions at the heterodimer interface, which are the determining factors for heat capacity change, are similar in magnitude.

Crystal structure of GBR2$_{VFT}$

Soluble GBR2$_{VFT}$ could be crystallized in two different forms (Supplementary Table 2 and 3; Supplementary Fig. 2). Form I crystals diffracted to 2.4 Å spacings. The structure was solved using a Pt derivative by single isomorphous replacement with anomalous scattering (SIRAS), and refined to an *R*-value of 20.1% (R_{free} = 21.7%). Form II crystals diffracted to 3.0 Å resolution. The structure was determined by molecular replacement using the form I GBR2$_{VFT}$ structure as the search model, and refined to a final *R*-factor of 21.0% (R_{free} = 25.7%).

The GBR2$_{VFT}$ crystal structure consists of two lobe-shaped domains (LB1 and LB2) connected by three short loops (Fig. 2a,b). Each domain has an αβ-fold composed of a central β-sheet flanked by α-helices. Overall, the molecule has an architecture similar to that found in mGluRs[5,8,9], natriuretic peptide receptors (NPR)[29–32], the N-terminal domain of ionotropic glutamate receptors[33], and bacterial periplasmic binding proteins (e.g., leucine/isoleucine/valine-binding protein[34].

A protein containing a VFT module can adopt an open or closed conformation, indicated by the hinge angle between its LB1 and LB2 domains. The closed conformation is often associated with agonist binding. Despite different crystal packing environments, the structure of GBR2$_{VFT}$ is very similar in both crystal forms, with an identical hinge angle (152°) (Supplementary Table 4). The LB1 domains can be superimposed with a root-mean-square deviation (RMSD) of 0.53 Å for 226 C_α atoms, and the LB2 domains with an RMSD of 0.31 Å for 177 C_α atoms. The conformational differences can be primarily attributed to a small change in their interdomain orientation, which corresponds to a 7.5°-twist around an axis that is roughly perpendicular to that of the domain closure.

Open conformation of GBR2$_{VFT}$ structure

At approximately 20% sequence identity, the extracellular domain of GBR2$_{VFT}$ has relatively low sequence homology to that of mGluRs. Nevertheless, GBR2$_{VFT}$ shares considerable structural homology with the known structures of mGluR1, mGluR3 and mGluR7[5,8,9]. The LB1 domains of GBR2$_{VFT}$ and mGluR1 can be superimposed with an RMSD of 1.5 Å for 176 C_α atoms, and the LB2 domains with an RMSD of 1.6 Å for 138 C_α atoms.

In comparison with known mGluR structures, GBR2$_{VFT}$ has an unusually large hinge angle (form I and II, 152°), suggesting an open conformation (Fig. 3). The difference between the interdomain angles of open (~135°) and closed (~110°) conformations of mGluRs is about 20–25°[5,8,9]. The hinge angle of GBR2$_{VFT}$ is more than 15° larger than the open conformation observed for free or antagonist-bound mGluR1 (Supplementary Table 4). A

structure-based sequence alignment shows that $GBR2_{VFT}$ has two insertions at the hinge region compared with mGluR structures (Supplementary Fig. 3). These include the loop between strand j and helix K in LB1 domain, and the β-hairpin loop between strands o and p in LB2. Residues from these regions form direct hydrogen bonds that bridge the LB1 and LB2 domains (Supplementary Fig. 3). These interdomain contacts may serve to stabilize the open conformation of $GBR2_{VFT}$. Although the insertions are expected to be present in the structure of $GBR1b_{VFT}$, residues forming the interdomain contacts in $GBR2_{VFT}$ are not conserved in $GBR1b_{VFT}$, thereby allowing $GBR1b_{VFT}$ to close upon agonist binding.

The GBR2 ectodomain differs from known mGluR structures in three other aspects (Fig. 2c). First, the structure of $GBR2_{VFT}$ features three disulfide bonds, two of which are conserved in the sequence of $GBR1b_{VFT}$. None of these are conserved in mGluRs. Second, mGluRs have a cysteine-rich region between the VFT and TM domain that is replaced by a 15- to 17-residue peptide linker in GBR1 and GBR2. Third, the structure of GBR2 $_{VFT}$ has several insertions and deletions compared with mGluR structures; many of these variations have no known biological implication. The most notable difference is the omission of a loop between helix B and strand c of $GBR2_{VFT}$ that, in mGluRs, is responsible for the formation of an intermolecular disulfide bond involved in dimerization. Consistent with this observation, $GABA_B$ receptor is a noncovalently-linked dimer, unlike mGluRs.

A Dali database search identified NPRs, particularly NPR-A, as the closest structural homologs to $GBR2_{VFT}$. The hinge angle between the LB1 and LB2 domains of NPRs is relatively invariant to the presence of ligand, possibly due to the location of ligand-binding site at the homodimeric interface instead of at the interdomain cleft. In addition, the presence of N-linked glycosylation at the cleft[29–32] may prevent domain closure. The hinge angle of NPR-A (141–142°) is closer to that of $GBR2_{VFT}$ than any known mGluR structure (Supplementary Table 4). Given the similarity between $GBR2_{VFT}$ and NPRs, and the non-ligand binding property of $GBR2_{VFT}$, the hinge angle of $GBR2_{VFT}$ may also remain constant throughout the resting and active states of $GABA_B$ receptor.

$GBR2_{VFT}$ closure not required for receptor activation

Sequence analysis revealed putative N-linked glycosylation sites at the interdomain cleft in chicken, honey bee, and *C. elegans* $GBR2_{VFT}$ (Supplementary Fig. 4), which may serve to prevent domain closure. Furthermore, $GBR2_{VFT}$ sequence identity across human, chicken, honey bee, and *C. elegans* ranges between 29.4% and 44.9%, suggesting structural conservation across species. Together, these data further suggest that human $GBR2_{VFT}$ perpetually adopts a rigid open conformation.

To investigate the functional relevance of a constitutively open $GBR2_{VFT}$, we introduced an N-linked glycosylation site at a prime $GBR2_{VFT}$ location (D256) in the interdomain cleft, a position which corresponds to a putative N-linked glycosylation site in honey bee GBR2 (Supplementary Fig. 4), hence likely to prevent any potential closure in GBR2. In order to accurately identify molecular weight changes, a truncated GBR2 mutant containing only the VFT module and a single TM helix ($GBR2_{VFT+TM1}$) was used for gel-shift analysis (Fig. 4a). Compared with wild-type $GBR2_{VFT+TM1}$, glycosylation mutant $GBR2_{VFT+TM1}$-N256 demonstrated reduced mobility on SDS PAGE, consistent with the presence of additional

carbohydrates at N256. Furthermore, this reduced mobility corresponds to the molecular weight of previously-characterized glycosylation mutant $GBR2_{VFT+TM1}$-N209[35]. In contrast, a Gln counterpart to the N209 mutant ($GBR2_{VFT+TM1}$-Q209) demonstrates a mobility similar to that of wild-type $GBR2_{VFT+TM1}$. Finally, treatment with the glycosidase PNGase F restored the gel mobility of the $GBR2_{VFT+TM1}$-N256 mutant to that of the wild-type $GBR2_{VFT+TM1}$ (Fig. 4b), demonstrating that the additional mass of $GBR2_{VFT+TM1}$-N256 was indeed due to glycosylation.

The functional consequences of this additional glycosylation at position 256 were evaluated via its effect on ligand-binding, G protein-coupling efficacy, and GIRK channel activation. The ligand-binding properties were measured by GABA- or $CGP54626_{ANT}$-inhibition of fluorescent $CGP54626_{ANT}$-red binding to the receptor. Co-expression of GBR2-N256 with wild-type GBR1 resulted in ligand-binding affinities indistinguishable from that of the wild-type heterodimer (Fig. 4c,d; Supplementary Table 5). In order to assay for changes in G protein coupling efficacy, GBR1 and GBR2 were co-expressed with chimeric $G_{\alpha qi9}$-protein, which allows for coupling to phospholipase C (PLC). GABA-induced inositol phosphate (IP) production was statistically the same for wild-type and mutant receptors, indicating that the presence of glycosylation at the cleft does not affect receptor function (Fig. 4e; Supplementary Table 5). Finally, in cells transfected with both GIRK (GIRK1 and GIRK2) and mutant $GABA_B$ receptor (GBR1b-wt and GBR2-N256), application of 100 μM GABA activated a large inward current (Fig. 4g). The magnitude of current potentiation was the same as that observed for wild-type receptor (Fig. 4f). Together, these results indicate that $GBR2_{VFT}$ closure is not required for receptor activation.

Mutational analyses of $GBR1_{VFT}$-$GBR2_{VFT}$ interface

Based on the structural homology of $GBR2_{VFT}$ to mGluRs, we have constructed models of the heterodimer in the resting state (open-open/R) and the putative asymmetric active state (closed-open/A), both featuring $GBR2_{VFT}$ in the open conformation (Fig. 5a,b). The dimer interface of $GABA_B$ receptor differs from that of mGluRs in its electrostatic property. The homodimer interface of mGluRs features a central hydrophobic core in both the active and resting states. In contrast, the $GBR2_{VFT}$ structure and $GBR1b_{VFT}$ model both exhibit scattered charged and hydrophobic regions, and appear to electrostatically complement one another (Fig. 5c,d). This indicates that the potential dimerization surface of $GABA_B$ is more polar than that of mGluRs overall.

To identify specific sites that are important for the heterodimeric interaction between $GBR1b_{VFT}$ and $GBR2_{VFT}$, we individually mutated a number of residues in the LB1 domain of each subunit that correspond to those located at the mGluR1 homodimer interface (Fig. 2c). We then investigated the effect of each mutation on $GABA_B$ signaling, and identified three tyrosine residues critical to agonist response.

The GBR2 residue Y118 is important for the activation of both GIRK channel and G_i protein. First, the single GBR2 mutation Y118A significantly decreased GABA-induced potentiation of GIRK current in HEK293 cells co-expressing the GIRK channel and $GABA_B$ receptor (Fig. 6a,b). Application of GABA to wild-type $GABA_B$ receptor at saturating concentrations resulted in the large expected increase in GIRK current density (Fig. 4f and

6b). In contrast, the GABA-induced increase mediated by the GBR2-Y118A mutant was only approximately 44% of the wild-type response. Second, the GBR2-Y118A mutation altered G_i activity (Fig. 6c). Transfection of HEK293 cells with wild-type $GABA_B$ receptor resulted in GABA-dependent stimulation of [^{35}S]-GTPγS binding, with a half-maximal effector concentration of 1.9 μM. Introducing the Y118A mutation to GBR2 reduced the maximum level of agonist-dependent [^{35}S]-GTPγS binding to 23% of that observed in wild-type. These observed effects of the GBR2 Y118A mutation were not due to reduced surface expression, as the level of cell-surface expression of GBR2-Y118A mutant was similar to that of wild-type GBR2, and, furthermore, it facilitated the surface transport of wild-type GBR1b (data not shown). The residual response of the mutant receptor in both functional assays may be attributed to a direct action of $GBR1b_{VFT}$ on GBR1 TM domain, which is in turn relayed to GBR2 TM domain[22]. Nevertheless, the reduced GIRK channel and G_i activities of the GBR2-Y118A mutant may likely reflect the impaired communication between GBR1 and GBR2 ectodomains.

Indeed, the Y118A mutation in $GBR2_{VFT}$ directly disrupts the interaction between $GBR2_{VFT}$ and $GBR1b_{VFT}$. The $GBR2_{VFT}$-Y118A mutant was expressed in baculovirus-infected insect cells and purified as a monomeric protein, indicating that the mutation does not affect the proper folding of $GBR2_{VFT}$. Using the SPA technique, we found that the $GBR2_{VFT}$-Y118A mutant had no effect on the GABA-binding affinity of $GBR1b_{VFT}$ (Fig. 6d). In contrast, wild-type $GBR2_{VFT}$ increased GABA-affinity by more than 6-fold (Fig. 1c). This indicates that Y118 of GBR2 is crucial for the heterodimeric interaction between $GBR1b_{VFT}$ and $GBR2_{VFT}$.

In addition to Y118 of GBR2, Y113 and Y117 of GBR1b also contribute to the heterodimeric interaction. Point mutation of Y113 to an alanine decreased agonist-induced [^{35}S]-GTPγS binding to 78% of the wild-type level (Fig. 7a). The effect of the single Y117A mutation was much more significant, with a GABA-stimulated [^{35}S]-GTPγS binding level that reached only 33% of wild-type (Fig. 7b). The partially-impaired function of each mutant cannot be attributed to reduced surface expression, since both were transported to the cell surface at levels comparable to wild-type GBR1b when co-expressed with wild-type GBR2 (data not shown). As observed with the GBR2-Y118A substitution, the GBR1b-Y113A and GBR1b-Y117A mutations most likely attenuated agonist-induced receptor function by weakening the heterodimeric interaction between the two subunits. In fact, all three tyrosine residues may participate in heterodimer formation through a combination of hydrophobic contacts and hydrogen-bonds.

Mutational analysis of ligand-binding site in $GBR1b_{VFT}$

The residues lining the interdomain cleft of GBR1 and mGluR ectodomains are conserved from *C. elegans* to human, consistent with their involvement in ligand recognition[24]. In contrast, the corresponding residues found in $GBR2_{VFT}$ are not conserved across species and their mutations do not affect receptor activation, consistent with the fact that $GBR2_{VFT}$ does not bind any known natural ligand[24]. Furthermore, none of the GBR1 residues critical for ligand binding are conserved in GBR2 (Fig. 2c).

Based on the GBR1b model, we identified residues at the interdomain cleft region that correspond to the ligand-binding site of mGluR1 (Fig. 2c). Some of the residues have been confirmed by previous mutagenesis studies to be important for ligand recognition, and these include S130, S153 and Y250[36,37]. In this study, we found that G151 of GBR1b is also part of this $GABA_B$ ligand-binding site (Supplementary Fig. 5). First, substitution of G151 with a valine residue essentially abolished binding by the competitive antagonist [^{3}H]-$CGP54626_{ANT}$ (Fig. 8a). Second, it caused drastic loss of receptor function, since no apparent simulation of [^{35}S]-GTPγS binding could be observed, even at saturating concentrations of GABA (Fig. 8b). The complete loss of function occurred despite the fact that the cell surface expression of the GBR1b-G151V mutant was comparable to that of wild-type receptor when co-expressed with wild-type GBR2 (data not shown). These observations indicate that G151 of GBR1b is directly involved in the recognition of both antagonist $CGP54626_{ANT}$ and agonist GABA, possibly through its main chain polar atoms. Mutation of G151 to a residue with a branched side chain, such as valine, may prevent the main chain atoms from being accessible to ligand.

DISCUSSION

The GBR2 ectodomain plays at least two important roles in the function of the heterodimeric $GABA_B$ receptor. First, the GBR2 ectodomain allosterically controls the agonist binding affinity of GBR1[11,14,22,25,26]. Second, it is required for efficient agonist-induced receptor activation[18,22]. Here we demonstrate that, through direct interaction with $GBR1b_{VFT}$, $GBR2_{VFT}$ potentiates agonist-binding by stabilizing the agonist-bound conformation of $GBR1_{VFT}$. We have determined the structure of $GBR2_{VFT}$, which reveals a polar heterodimer interface, unlike the hydrophobic homodimer interface of mGluRs. Because of their high sequence homology, $GBR2_{VFT}$ provides an excellent template for modeling the structure of $GBR1b_{VFT}$. These structural models have allowed us to identify residues from both subunits that are important for heterodimerization, and GBR1b residues that are involved in ligand recognition. Furthermore, we provide structural and functional evidence of a constitutively open $GBR2_{VFT}$, which suggests structural asymmetry in the active state of the $GABA_B$ receptor ectodomain.

Previously, time-resolved fluorescent resonance energy transfer (TR-FRET) techniques have demonstrated that GBR1 and GBR2 ectodomains come within close proximity[25]. Additionally, the GBR1 ectodomain is able to pull down the GBR2 ectodomain, and their mixture shifts sucrose gradient sedimentation[26]. Here we provide evidence of direct binding between $GBR1b_{VFT}$ and $GBR2_{VFT}$ with a 1:1 stoichiometry. We also confirm previous results indicating that GBR2 increases the agonist-binding affinity of GBR1. It has been suggested that this increased affinity occurs by one or both of two mechanisms: either GBR2 directly acts on the ectodomain of GBR1, or it prevents the inhibitory interaction of the GBR1 ectodomain and GBR1 TM domain[25]. By measuring the strength of $GBR1_{VFT}$-$GBR2_{VFT}$ interaction in the presence of agonist and antagonist, our calorimetry and binding data support the previous hypothesis that the direct contact between GBR1 and GBR2 ectodomains enhances agonist affinity by selectively stabilizing the agonist-bound conformation of GBR1[25].

It is not known whether $GBR2_{VFT}$ can spontaneously open and close. Our structural data suggests that the open conformation of $GBR2_{VFT}$ is likely to be relatively rigid for four reasons. First, $GBR2_{VFT}$ has an identical hinge angle within two different crystal packing environments, suggesting that the open conformation may be the thermodynamically favored state of $GBR2_{VFT}$. Second, the open conformation of $GBR2_{VFT}$ is stabilized by interdomain hydrogen bonds in the cleft region. Third, the closed conformation is often associated with ligand-binding, and $GBR2_{VFT}$ is not known to bind any natural ligand[24]. Fourth, the closest structural homolog of $GBR2_{VFT}$, NPR-A, has a constitutively open conformation in the absence and presence of ligand, possibly due to the presence of carbohydrates at the cleft[31,32].

We have, furthermore, demonstrated that $GBR2_{VFT}$ closure is not required for receptor activation. Sequence analysis identified three eukaryotic GBR2 subunits significantly similar to human GBR2, which contain native glycosylation sites in the interdomain cleft. Since the structure of $GBR2_{VFT}$ is likely to be conserved across species, the presence of putative glycosylation sites suggests that the open conformation observed in human $GBR2_{VFT}$ is rigid. We investigated the functional relevance of a constitutively open $GBR2_{VFT}$ by blocking any potential closure via insertion of a large glycan at the cleft. This prevention of $GBR2_{VFT}$ closure had no effect on ligand-binding affinity or G protein coupling efficacy, further indicating that $GBR2_{VFT}$ adopts a constitutively open conformation.

The constitutively open conformation of $GBR2_{VFT}$ suggests that the ectodomain of $GABA_B$ receptor functions in an asymmetric way. Specifically, we propose that both $GBR1b_{VFT}$ and $GBR2_{VFT}$ are in an open conformation in the resting state and that only $GBR1b_{VFT}$ closes upon ligand-induced activation. FRET data suggest that the intracellular loops of the $GABA_B$ receptor TM domain also undergo asymmetrical intersubunit rearrangement upon activation[38]. Indeed, direct allosteric interactions between the TM domains of the two subunits have been shown to take part in signal transduction[22]. An asymmetrical activated dimer has also been observed for a number of class A and class C GPCRs[39]. For example, the minimal signaling unit of dopamine D2 receptors consists of two receptors and one G protein, with maximal signaling achieved by agonist binding to a single protomer[40]. Class C GPCRs are known to function either as homodimers linked by a disulfide bridge or obligatory heterodimers. Structural data obtained for the extracellular ligand-binding domain of mGluR1 indicates that closure of one protomer is sufficient to induce the active conformation of the homodimer although full activation requires the closure of both ectodomains[5,7]. Data on positive allosteric modulators (PAM) of mGluRs further demonstrates that a single TM domain per dimer reaches the active state during receptor activation[41].

Two models have been proposed for the mechanism of $GABA_B$ receptor activation. One model suggests that receptor activation is mediated without higher-order rearrangements, by signals relayed within each protomer via direct contacts between the VFT and TM domains. This model is supported by the observation that the peptide linker between the VFT and TM domains can tolerate variations in sequence and length[42]. A second model proposes that the activation mechanism of $GABA_B$ receptor resembles that of mGluRs[4]. Specifically, ligand

binding induces a reorientation of the ectodomains of GBR1 and GBR2 relative to each other, thereby bringing the TM domains of the two subunits together to trigger G protein coupling[22]. Both structural and biochemical evidence point to a rather rigid architecture for the GBR2 ectodomain, which precludes a ligand-induced intramolecular conformational change involving VFT closure. Receptor activation would then depend on higher-order rearrangements between GBR1 and GBR2, such as a re-orientation of the dimer interface. This supports a signal transduction mechanism similar to that of mGluRs, indicating that G protein signaling in the major excitatory and inhibitory neurotransmission systems (i.e., the glutamatergic and GABAergic systems) involves architectural rearrangements of extracellular domains. It is of note, however, that the constitutively open conformation of the modulatory subunit of $GABA_B$ receptor is unique to the inhibitory GABAergic system (Fig. 5a,b).

METHODS

Protein expression and purification

The ectodomains of human GBR1 and GBR2 were separately cloned into a pFastBac vector (Invitrogen) for expression. GBR1 has two major isoforms GBR1a and GBR1b[28]. $GBR1b_{VFT}$ contained residues 30–459 with the signal peptide of baculovirus glycoprotein gp67 attached at the N-terminus and a Flag tag at the C-terminus. $GBR1b_{VFT}$His included an additional C-terminal His tag. $GBR2_{VFT}$ contained residues 1–466 and a C-terminal Flag tag. $GBR2_{VFT}$-Y118A had a single mutation Y118A.

Sf9 insect cells were infected with recombinant baculovirus carrying the $GBR1b_{VFT}$ or $GBR2_{VFT}$ gene. The target protein was purified from cell supernatant using an anti-Flag antibody (M2) affinity column followed by gel filtration chromatography. $GBR1b_{VFT}$ was produced in the absence and presence of various ligands (100 μM GABA, 1 μM $SKF97541_{AGO}$, and 10 μM $CGP54626_{ANT}$); each ligand was present throughout expression.

Crystallization and data collection

$GBR2_{VFT}$ was crystallized in two different forms at 20°C. Form I crystals were grown in 18% polyethylene glycol monomethyl ether 550, 20% glycerol, 2 mM $ZnSO_4$, and 0.1 M Na cacodylate, pH 6.5, and directly frozen from drops. Diffraction data were measured at 24ID-C beamline of Advanced Photon Source (APS). A native data set was collected to 2.4 Å. A Pt-derivative was obtained by soaking crystals with 5mM K_2PtCl_4; its diffraction extended to 3.8 Å.

Form II crystals were obtained from 30% Jeffamine ED-2001, and 0.1M HEPES, pH 7.0. The crystals were soaked in a cryoprotectant containing 20% PEG400 and reservoir solution, then flash-cooled with liquid nitrogen. A native data set was collected to 3.0 Å at X4C beamline of National Synchrotron Light Source (NSLS).

Structure determination

The structure of $GBR2_{VFT}$ in crystal form I was solved by single isomorphous replacement with anomalous scattering (SIRAS). The positions of Pt atoms in the derivative crystal were

located with HKL2MAP[43] using anomalous differences of Pt atoms at the LIII edge (1.072 Å). Refinement of heavy atom parameters, phase calculation, and density modification were performed with SHARP[44] at 50–3.8 Å, using both anomalous and isomorphous differences from the native and derivative data sets. Based on the 3.8 Å SIRAS maps, we traced the backbone of $GBR2_{VFT}$ with COOT. This initial model was refined against the native data to 2.4 Å using BUSTER[45]. A complete atomic model of $GBR2_{VFT}$ was developed through iterative model building and refinement. The last stages of refinement were carried out in REFMAC[46].

The final model of $GBR2_{VFT}$ contains protein residues 52–293 and 300–466, the entire C-terminal Flag tag, 1 N-acetylglucosamine, 1 fucose, 2 Zn^{2+} ions, and 142 water molecules. Ramachandran analysis performed with MolProbity[47] places 97.3% of all residues in favored regions and 0.24% in outlier regions.

The form II structure was solved by molecular replacement using the form I structure as the search model. Refinement was carried out in BUSTER[45] and at the last stages in REFMAC[46]. The final structure contains $GBR2_{VFT}$ residues 49–293 and 302–466, 5 N-acetylglucosamines, 1 fucose, and 96 water molecules. Geometric analysis using MolProbity[47] places 95.1% of all residues in favored regions and 1.2% as outliers.

Structural analysis and homology modeling

The interdomain hinge angle is defined as the angle formed by the centers of mass of LB1 and LB2 domains about a central pivot point in the interdomain linker region. The center of mass for each domain was calculated using the TABFUN function of AMoRE[48].

A homology model was created for $GBR1b_{VFT}$ based on the $GBR2_{VFT}$ structure using Modeller[49]. The open conformation of $GBR1b_{VFT}$ was generated by superimposing its LB1 and LB2 domains separately onto the structure of an open conformer of mGluR1 (1EWT, B chain)[5]. The closed conformation of $GBR1b_{VFT}$ was generated similarly using a closed conformer of mGluR1 (1EWK, A chain)[5]. The structure of free mGluR1 (1EWT)[5] served as a template to model the resting state of a $GBR1b_{VFT}$-$GBR2_{VFT}$ heterodimer, with both $GBR1b_{VFT}$ and $GBR2_{VFT}$ in the open conformation (Open-Open/R). The structure of glutamate-bound mGluR1 (1EWK)[5] was used to model the active state, with GBR1b in the closed conformation and GBR2 in the open conformation (Closed-Open/A).

Scintillation proximity assay

Yttrium silicate (YSI) Cu^{2+} His-tag SPA beads (PerkinElmer) (250 μg) were added to $GBR1b_{VFT}$His (0.5 μg), a mixture of $GBR1b_{VFT}$His (0.5 μg) and $GBR2_{VFT}$ (1.0 μg), or a mixture of $GBR1b_{VFT}$His (0.5 μg) and $GBR2_{VFT}$-Y118A (1.0 μg) pre-incubated with 100 nM [^{3}H]-GABA (35 Ci/mmol) at 4°C. Increasing concentrations of non-radioactive GABA, $baclofen_{AGO}$, $SKF97541_{AGO}$, or $CGP54626_{ANT}$ were added to compete for receptor binding. Each reaction was also performed in the presence of 800 mM imidazole for background correction. The plates were counted in a Microbeta counter (PerkinElmer). Data were analyzed using the non-linear regression algorithms in Prism (GraphPad).

Isothermal titration calorimetry

The titration calorimetry experiments were carried out in an ITC-200 calorimeter (MicroCal) at 15°C. $GBR1b_{VFT}$-$SKF97541_{AGO}$ protein was placed in the sample cell at 19.35 μM, and $GBR2_{VFT}$ was added from a 81.65 μM stock in 1.5 μl injections. The titration was carried out until $GBR1b_{VFT}$-$SKF97541_{AGO}$ was saturated with $GBR2_{VFT}$. Similarly, $GBR1b_{VFT}$-$CGP54626_{ANT}$ was placed in the sample cell at 13.91 μM, and titrated with 1.5 μl-injections of 52.24 μM $GBR2_{VFT}$. For each titration, the heat effects of buffer dilution were measured in a control experiment where the $GBR2_{VFT}$ protein was titrated into the buffer following the same injection schedule as the sample titration. Data were analyzed using MicroCal Origin. After subtracting the control data, the sample titration was fit to a single binding-site model.

Differential scanning calorimetry

Temperature-induced protein unfolding of $GBR1b_{VFT}$-$SKF97541_{AGO}$ and $GBR1b_{VFT}CGP54626_{ANT}$ were measured using a VP-Capillary differential scanning calorimeter (DSC) (MicroCal) at a heating rate of 2°K/min. The thermal transition midpoint (T_m) of $GBR1b_{VFT}$-$SKF97541_{AGO}$ and $GBR1b_{VFT}$-$CGP54626_{ANT}$ were measured at protein concentrations of 11.58 μM and 25.65 μM, respectively. Data were analyzed with MicroCal Origin.

Western blot

A truncated GBR2 subunit containing only the VFT module and first TM helix ($GBR2_{VFT+TM1}$) was subcloned into a pRK5 vector with an N-terminal HA tag. The $GBR2_{VFT+TM1}$-N256 mutant contained mutations D256N and N258S. The mutant $GBR2_{VFT+TM1}$-N209 carries mutations S209N and V211S, and $GBR2_{VFT+TM1}$-Q209 carries mutations S209Q and V211S[35].

Human embryonic kidney (HEK293) cells transfected with each plasmid were harvested to obtain the membrane fraction. Deglycosylation of $GBR2_{VFT+TM1}$ and $GBR2_{VFT+TM1}$-N256 was carried out using PNGase F (Roche) under denaturing conditions. Western blot analysis was performed using a rabbit polyclonal anti-HA antibody (Life technologies)[24]. Proteins were visualized by electrochemiluminescence.

Inositol phosphate (IP) measurement

Wild-type full-length GBR1a (GBR1a-wt) tagged at its N-terminal end with a Flag epitope followed by a snap-tag was inserted into a pRK5 plasmid[50]. Similarly, pRK5 plasmids containing wild-type full-length GBR2 (GBR2-wt)[18,35] and a glycosylation mutant (GBR2-N256, with mutations D256N and N258S) tagged at their N-terminal ends with an HA epitope were generated.

Measurement of IP accumulation was carried out as described[51] using HEK293 cells co-transfected with GBR1a-wt, GBR2-wt or GBR2-N256, and $G_{\alpha qi9}$. Briefly, after labeling with [^{3}H]myo-inositol, cells were stimulated with or without ligand. The IP produced were purified by ion-exchange chromatography. Radioactivity was measured using a MicroBeta counter. Results are expressed as the ratio between IP and the total radioactivity present in

the membranes and normalized to the maximal stimulation. Data were analyzed using the non-linear regression algorithms in Prism.

Competition binding assay

Competition binding assays were performed with Tag-lite™ technology (Cisbio) on intact HEK293 cells co-transfected with GBR1a-wt and GBR2-wt or GBR2-N256. The cells were labeled with 100 nM SNAP-Lumi4Tb, and then incubated with increasing concentrations of a non-fluorescent ligand (GABA or $CGP54626_{ANT}$) and 5 nM of fluorescent $CGP54626_{ANT}$-red. The fluorescence was collected at 620 and 665 nm using a Rubystar plate reader (BMG Labtech), 50 ms after laser excitation at 337 nm. The FRET signal was calculated as the ratio $(signal_{665\ nm}) / (signal_{620\ nm}) \times 10^4$ and plotted against the concentration of non-fluorescent ligand. Non-specific binding was determined in the presence of 1 μM unlabeled $CGP54626_{ANT}$. Data were analyzed using the non-linear regression algorithms in Prism. K_i was calculated according to the equation $K_i = IC_{50} \times K_d / (K_d + [L])$, where K_d is the dissociation constant of $CGP54626_{ANT}$-red, $[L]$ is the concentration of $CGP54626_{ANT}$-red and IC_{50} is experimentally defined.

Cell surface expression

Wild-type and mutants of full-length GBR1b and GBR2 in pcDNA3.1(+) (Invitrogen) were constructed using QuikChange (Stratagene). A Flag tag was inserted after the signal peptide of GBR1b, and an HA tag was placed after the signal peptide of GBR2.

HEK 293T/17 cells (ATCC) were co-transfected with GBR1b and GBR2. We used cells permeabilized with 0.5% Triton X100 to determine the total expression level of GBR1b and GBR2 in transfected cells. Untreated cells were used to determine the cell surface expression level of each subunit.

After blocking with milk, the cells were incubated with primary antibody. Mouse anti-Flag M1 antibody (Sigma) was used to detect GBR1b expression. Mouse anti-HA antibody HA. 11 clone 16B12 (Covance) was used to measure GBR2 expression levels. Both were followed by donkey anti-mouse IRDye 800-labeled antibody (LiCor) as the secondary antibody. Fluorescent signals were measured using an Odyssey Infrared Imager (LiCor). The results of three independent experiments were used for statistical analysis.

Electrophysiology

HEK293 T/17 cells were transiently transfected with human GBR1b and GBR2, mouse GIRK1 and GIRK2, and GFP. Currents were measured in the whole-cell configuration using an Axopatch 200B amplifier (Axon Instruments).

The internal pipette solution for patch clamping contained 110 mM K-aspartate, 5 mM ATP-K_2, 11 mM EGTA, 10 mM HEPES, 5.5 mM $CaCl_2$, and 1 mM $MgCl_2$, pH 7.3. Seal formation and cell membrane rupture were completed in a low potassium external solution containing 132 mM NaCl, 4.8 mM KCl, 1.2 mM $MgCl_2$, 2 mM $CaCl_2$, 5 mM glucose, and 10 mM Hepes, pH 7.4. After membrane rupture, the external solution was switched to a high

potassium solution containing 135 mM KCl, 1.2 mM $MgCl_2$, 2 mM $CaCl_2$, 5 mM glucose, and 10 mM Hepes, pH 7.4.

The baseline GIRK rectification was measured in the absence of GABA. Briefly, from a holding potential of 10 mV (the reversal potential), the membrane voltage was stepped at 500 ms pulses from –100 mV to 40 mV in 20 mV increments. The current for each step was calculated as the average of the data acquired during the last 100 ms of each pulse. To obtain the effect of GABA, the cells were perfused with different concentrations of GABA (from 1 μM to 1 mM) in high potassium solution. The current-voltage (I-V) relationship was assessed in the presence of the agonist following the same protocol as for basal current measurement. For statistical comparisons, we used the percentage increase in current density measured at −80 mV during the perfusion. Patch clamp data was acquired using pClamp8 (Axon Instruments). Analysis was performed using MicroCal Origin.

Agonist-stimulated [^{35}S]-GTPγS binding

HEK293 T/17 cells were transiently transfected with full-length GBR1b and GBR2. Harvested cell membranes were suspended in 50 mM Tris pH 7.7, 100 mM NaCl, 12 mM $MgCl_2$, 1.8 mM $CaCl_2$, and 0.2 mM EGTA to approximately 400 μg protein per ml. The membrane homogenates were incubated with increasing concentrations of GABA and 10 μM GDP. [^{35}S]-GTPγS (1250 Ci/mmol) was then added to a final concentration of 0.5 nM. Unbound [^{35}S]-GTPγS was removed by centrifugation. The amount of bound [^{35}S]-GTPγS was measured using a Beckman liquid scintillation counter. Nonspecific binding was measured in the presence of 20 μM unlabeled GTPγS. Basal activity was determined in the absence of GABA. Data analysis was performed using the non-linear regression algorithms in Prism.

Radioligand binding assay

HEK293 T/17 cells were transiently transfected with full-length human GBR1b and GBR2. Cell membranes were suspended in 20 mM Tris pH 7.4, 118 mM NaCl, 5.6 mM glucose, 1.2 mM KH_2PO_4, 1.2 mM $MgSO_4$, 4.7 mM KCl, and 1.8 mM $CaCl_2$ to approximately 400 μg protein per ml. [^{3}H]-CGP54626$_{ANT}$ (25 Ci/mmol) was added to the reaction mixture to final concentrations ranging from 0.5 nM to 20 nM. Unbound [^{3}H]-CGP54626$_{ANT}$ was removed by centrifugation. The amount of bound [^{3}H]-CGP54626$_{ANT}$ was measured by liquid scintillation counting. Nonspecific binding was measured in the presence of 10 mM unlabeled GABA. Data analysis was performed using the non-linear regression algorithms in Prism.

Supplementary Material

Refer to Web version on PubMed Central for supplementary material.

ACKNOWLEDGEMENTS

We thank Dr. W.A. Hendrickson for advice and generously providing lab space at the initial stage of this project, Dr. R. Kass for support and advice on electrophysiology experiments, Dr. L. Jan for the cDNA clones of GIRK channels, Dr. V. Frasca for ITC and DSC measurements, Drs. C. Brouillette and I. Protassevitch for DSC measurements, Drs. L. Shapiro and J. Hunt for advice, M. Gawinowicz for mass spectrometry and protein

sequencing, Drs. K. Rajashankar at APS and J. Schwanof at NSLS for help with data collection, L. Geneve for analyzing the glycosylation mutants, ARPEGE platform facility at Institute of Functional Genomics (Montpellier, France) for IP and Tag Lite® assays, Drs. W.A. Hendrickson and M. Evelyn for critical reading of the manuscript. This work was supported by the AHA Grant SDG0835183N, NIH Grant R01GM088454 (both to Q.R.F.), and ANR grant ANR-09-BLANC-0272 (to J.P.P.). Q.R.F. is an Irma Hirschl Career Scientist, Pew Scholar and McKnight Scholar.

REFERENCES

1. Macdonald RL, Olsen RW. GABAA receptor channels. Annu Rev Neurosci. 1994; 17:569–602. [PubMed: 7516126]
2. Bettler B, Kaupmann K, Mosbacher J, Gassmann M. Molecular structure and physiological functions of GABA(B) receptors. Physiol Rev. 2004; 84:835–867. [PubMed: 15269338]
3. Bowery NG, et al. International Union of Pharmacology. XXXIII. Mammalian gamma-aminobutyric acid(B) receptors: structure and function. Pharmacol Rev. 2002; 54:247–264. [PubMed: 12037141]
4. Pin JP, et al. The activation mechanism of class-C G protein coupled receptors. Biol Cell. 2004; 96:335–342. [PubMed: 15207901]
5. Kunishima N, et al. Structural basis of glutamate recognition by a dimeric metabotropic glutamate receptor. Nature. 2000; 407:971–977. [PubMed: 11069170]
6. Tsuji Y, et al. Cryptic dimer interface and domain organization of the extracellular region of metabotropic glutamate receptor subtype 1. J Biol Chem. 2000; 275:28144–28151. [PubMed: 10874032]
7. Kniazeff J, et al. Closed state of both binding domains of homodimeric mGlu receptors is required for full activity. Nat Struct Mol Biol. 2004; 11:706–713. [PubMed: 15235591]
8. Muto T, Tsuchiya D, Morikawa K, Jingami H. Structures of the extracellular regions of the group II/III metabotropic glutamate receptors. Proc Natl Acad Sci U S A. 2007; 104:3759–3764. [PubMed: 17360426]
9. Tsuchiya D, Kunishima N, Kamiya N, Jingami H, Morikawa K. Structural views of the ligand-binding cores of a metabotropic glutamate receptor complexed with an antagonist and both glutamate and Gd3+ Proc Natl Acad Sci U S A. 2002; 99:2660–2665. [PubMed: 11867751]
10. Jones KA, et al. GABA(B) receptors function as a heteromeric assembly of the subunits GABA(B)R1 and GABA(B)R2. Nature. 1998; 396:674–679. [PubMed: 9872315]
11. Kaupmann K, et al. GABA(B)-receptor subtypes assemble into functional heteromeric complexes. Nature. 1998; 396:683–687. [PubMed: 9872317]
12. Kuner R, et al. Role of heteromer formation in GABAB receptor function. Science. 1999; 283:74–77. [PubMed: 9872744]
13. Ng GY, et al. Identification of a GABAB receptor subunit, gb2, required for functional GABAB receptor activity. J Biol Chem. 1999; 274:7607–7610. [PubMed: 10075644]
14. White JH, et al. Heterodimerization is required for the formation of a functional GABA(B) receptor. Nature. 1998; 396:679–682. [PubMed: 9872316]
15. Milligan G. G protein-coupled receptor hetero-dimerization: contribution to pharmacology and function. Br J Pharmacol. 2009; 158:5–14. [PubMed: 19309353]
16. Margeta-Mitrovic M, Jan YN, Jan LY. A trafficking checkpoint controls GABA(B) receptor heterodimerization. Neuron. 2000; 27:97–106. [PubMed: 10939334]
17. Duthey B, et al. A single subunit (GB2) is required for G protein activation by the heterodimeric GABA(B) receptor. J Biol Chem. 2002; 277:3236–3241. [PubMed: 11711539]
18. Galvez T, et al. Allosteric interactions between GB1 and GB2 subunits are required for optimal GABA(B) receptor function. EMBO J. 2001; 20:2152–2159. [PubMed: 11331581]
19. Havlickova M, et al. The intracellular loops of the GB2 subunit are crucial for G protein coupling of the heteromeric gamma-aminobutyrate B receptor. Mol Pharmacol. 2002; 62:343–350. [PubMed: 12130687]
20. Margeta-Mitrovic M, Jan YN, Jan LY. Function of GB1 and GB2 subunits in G protein coupling of GABA(B) receptors. Proc Natl Acad Sci U S A. 2001; 98:14649–14654. [PubMed: 11724956]

21. Robbins MJ, et al. GABA(B2) is essential for G protein coupling of the GABA(B) receptor heterodimer. J Neurosci. 2001; 21:8043–8052. [PubMed: 11588177]
22. Monnier C, et al. Trans-activation between 7TM domains: implication in heterodimeric GABA(B) receptor activation. EMBO J. 2011; 30:32–42. [PubMed: 21063387]
23. Malitschek B, et al. The N-terminal domain of gamma-aminobutyric Acid(B) receptors is sufficient to specify agonist and antagonist binding. Mol Pharmacol. 1999; 56:448–454. [PubMed: 10419566]
24. Kniazeff J, Galvez T, Labesse G, Pin JP. No ligand binding in the GB2 subunit of the GABA(B) receptor is required for activation and allosteric interaction between the subunits. J Neurosci. 2002; 22:7352–7361. [PubMed: 12196556]
25. Liu J, et al. Molecular determinants involved in the allosteric control of agonist affinity in the GABAB receptor by the GABAB2 subunit. J Biol Chem. 2004; 279:15824–15830. [PubMed: 14736871]
26. Nomura R, Suzuki Y, Kakizuka A, Jingami H. Direct detection of the interaction between recombinant soluble extracellular regions in the heterodimeric metabotropic gamma-aminobutyric acid receptor. J Biol Chem. 2008; 283:4665–4673. [PubMed: 18165688]
27. Quick M, Javitch JA. Monitoring the function of membrane transport proteins in detergent-solubilized form. Proc Natl Acad Sci U S A. 2007; 104:3603–3608. [PubMed: 17360689]
28. Kaupmann K, et al. Expression cloning of GABA(B) receptors uncovers similarity to metabotropic glutamate receptors. Nature. 1997; 386:239–246. [PubMed: 9069281]
29. He X, Chow D, Martick MM, Garcia KC. Allosteric activation of a spring-loaded natriuretic peptide receptor dimer by hormone. Science. 2001; 293:1657–1662. [PubMed: 11533490]
30. He XL, Dukkipati A, Garcia KC. Structural determinants of natriuretic peptide receptor specificity and degeneracy. J Mol Biol. 2006; 361:698–714. [PubMed: 16870210]
31. Ogawa H, Qiu Y, Ogata CM, Misono KS. Crystal structure of hormone-bound atrial natriuretic peptide receptor extracellular domain: rotation mechanism for transmembrane signal transduction. J Biol Chem. 2004; 279:28625–28631. [PubMed: 15117952]
32. van den Akker F, et al. Structure of the dimerized hormone-binding domain of a guanylyl-cyclase-coupled receptor. Nature. 2000; 406:101–104. [PubMed: 10894551]
33. Armstrong N, Sun Y, Chen GQ, Gouaux E. Structure of a glutamate-receptor ligand-binding core in complex with kainate. Nature. 1998; 395:913–917. [PubMed: 9804426]
34. Sack JS, Saper MA, Quiocho FA. Periplasmic binding protein structure and function. Refined X-ray structures of the leucine/isoleucine/valine-binding protein and its complex with leucine. J Mol Biol. 1989; 206:171–191. [PubMed: 2649682]
35. Rondard P, et al. Functioning of the dimeric GABA(B) receptor extracellular domain revealed by glycan wedge scanning. EMBO J. 2008; 27:1321–1332. [PubMed: 18388862]
36. Galvez T, et al. Mutagenesis and modeling of the GABAB receptor extracellular domain support a venus flytrap mechanism for ligand binding. J Biol Chem. 1999; 274:13362–13369. [PubMed: 10224098]
37. Galvez T, et al. Mapping the agonist-binding site of GABAB type 1 subunit sheds light on the activation process of GABAB receptors. J Biol Chem. 2000; 275:41166–41174. [PubMed: 10986293]
38. Matsushita S, Nakata H, Kubo Y, Tateyama M. Ligand-induced rearrangements of the GABA(B) receptor revealed by fluorescence resonance energy transfer. J Biol Chem. 2010; 285:10291–10299. [PubMed: 20129919]
39. Rovira X, Pin JP, Giraldo J. The asymmetric/symmetric activation of GPCR dimers as a possible mechanistic rationale for multiple signalling pathways. Trends Pharmacol Sci. 2010; 31:15–21. [PubMed: 19963287]
40. Han Y, Moreira IS, Urizar E, Weinstein H, Javitch JA. Allosteric communication between protomers of dopamine class A GPCR dimers modulates activation. Nat Chem Biol. 2009; 5:688–695. [PubMed: 19648932]
41. Goudet C, et al. Asymmetric functioning of dimeric metabotropic glutamate receptors disclosed by positive allosteric modulators. J Biol Chem. 2005; 280:24380–24385. [PubMed: 15863499]

42. Margeta-Mitrovic M, Jan YN, Jan LY. Ligand-induced signal transduction within heterodimeric GABA(B) receptor. Proc Natl Acad Sci U S A. 2001; 98:14643–14648. [PubMed: 11724957]

METHODS REFERENCES

43. Pape T, Schneider TR. HKL2MAP: a granphical user interface for phasing with SHELX programs. J Appl Cryst. 2004; 37:843–844.

44. De la Fortelle E, Bricogne G. Maximum-likelihood heavy-atom parameter refinement for multiple isomorphous replacement and multiwavelength anomalous diffraction methods. Methods Enzymol. 1997; 276:472–494.

45. Roversi P, Blanc E, Vonrhein C, Evans G, Bricogne G. Modelling prior distributions of atoms for macromolecular refinement and completion. Acta Crystallogr D Biol Crystallogr. 2000; 56:1316–1323. [PubMed: 10998628]

46. Murshudov GN, Vagin AA, Dodson EJ. Refinement of macromolecular structures by the maximum–likelihood method. Acta Crystallogr D Biol Crystallogr. 1997; 53:240–255. [PubMed: 15299926]

47. Chen VB, et al. MolProbity: all-atom structure validation for macromolecular crystallography. Acta Crystallogr D Biol Crystallogr. 2010; 66:12–21. [PubMed: 20057044]

48. Navaza J. Implementation of molecular replacement in AMoRe. Acta Crystallogr D Biol Crystallogr. 2001; 57:1367–1372. [PubMed: 11567147]

49. Eswar N, Eramian D, Webb B, Shen MY, Sali A. Protein structure modeling with MODELLER. Methods Mol Biol. 2008; 426:145–159. [PubMed: 18542861]

50. Maurel D, et al. Cell-surface protein-protein interaction analysis with time-resolved FRET and snap-tag technologies: application to GPCR oligomerization. Nat Methods. 2008; 5:561–567. [PubMed: 18488035]

51. Kniazeff J, et al. Locking the dimeric GABA(B) G protein-coupled receptor in its active state. J Neurosci. 2004; 24:370–377. [PubMed: 14724235]

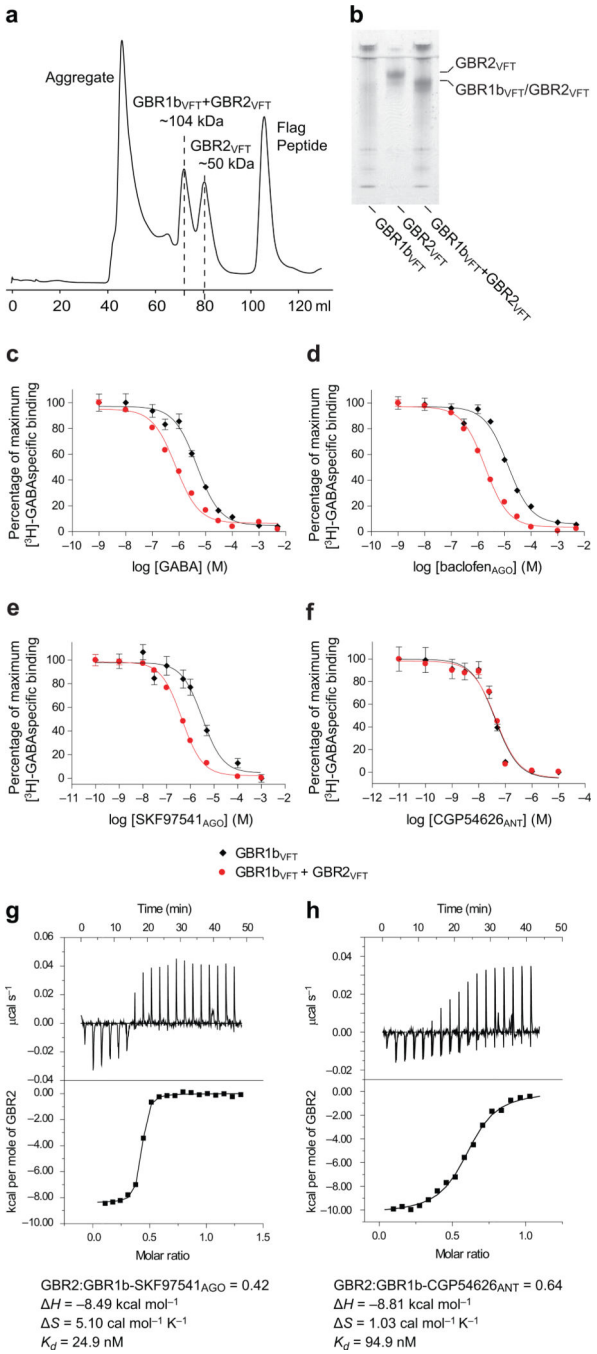

Figure 1. Interaction between GBR1b$_{VFT}$ and GBR2$_{VFT}$

(a) Superdex 200 gel filtration chromatography of a mixture of GBR1b$_{VFT}$ and GBR2$_{VFT}$.

(b) Native gel electrophoresis (8–25%) demonstrating the complex formation between GBR1b$_{VFT}$ and GBR2$_{VFT}$. Lane 1 is GBR1$_{VFT}$, lane 2 is GBR2$_{VFT}$, and lane 3 contains a mixture of GBR1$_{VFT}$ and GBR2$_{VFT}$.

(c–f) Dose-response curves of agonists (c) GABA, (d) baclofen$_{AGO}$ and (e) SKF97541$_{AGO}$, and (f) antagonist CGP54626$_{ANT}$ inhibiting [^{3}H]-GABA binding to GBR1b$_{VFT}$. Each reaction was carried out in the absence (black) or presence (red) of GBR2$_{VFT}$. The specific

binding in the absence and presence of $GBR2_{VFT}$ was approximately 75% and 90% of the total binding, respectively. Data points represent mean ± s.e.m. of triplicate measurements. (g,h) Thermodynamics of the interactions between (g) $GBR2_{VFT}$ and $GBR1b_{VFT}$-$SKF97541_{AGO}$ or (h) $GBR2_{VFT}$ and $GBR1b_{VFT}$-$CGP54626_{ANT}$. Each panel presents raw data (top) and heat data after peak integration and subtraction of control titration (bottom). Heat changes are plotted as a function of the molar ratio of $GBR2_{VFT}$ to $GBR1b_{VFT}$ for each injection. Curve represents the best non-linear least-squares fitting of the data to a one-site binding model. The enthalpy change (ΔH), entropy change (ΔS), stoichiometry and dissociation constant (K_d) of each reaction correspond to mean values of two experiments. The binding stoichiometry between $GBR2_{VFT}$ and $GBR1b_{VFT}$ was much lower than the 1:1 ratio expected from a heterodimeric complex. One possible explanation is that only a fraction of $GBR1b_{VFT}$-$SKF97541_{AGO}$ (42%) and $GBR1b_{VFT}$-$CGP54626_{ANT}$ (64%) were properly folded. A second possibility is that the binding kinetics involves a fast off-rate.

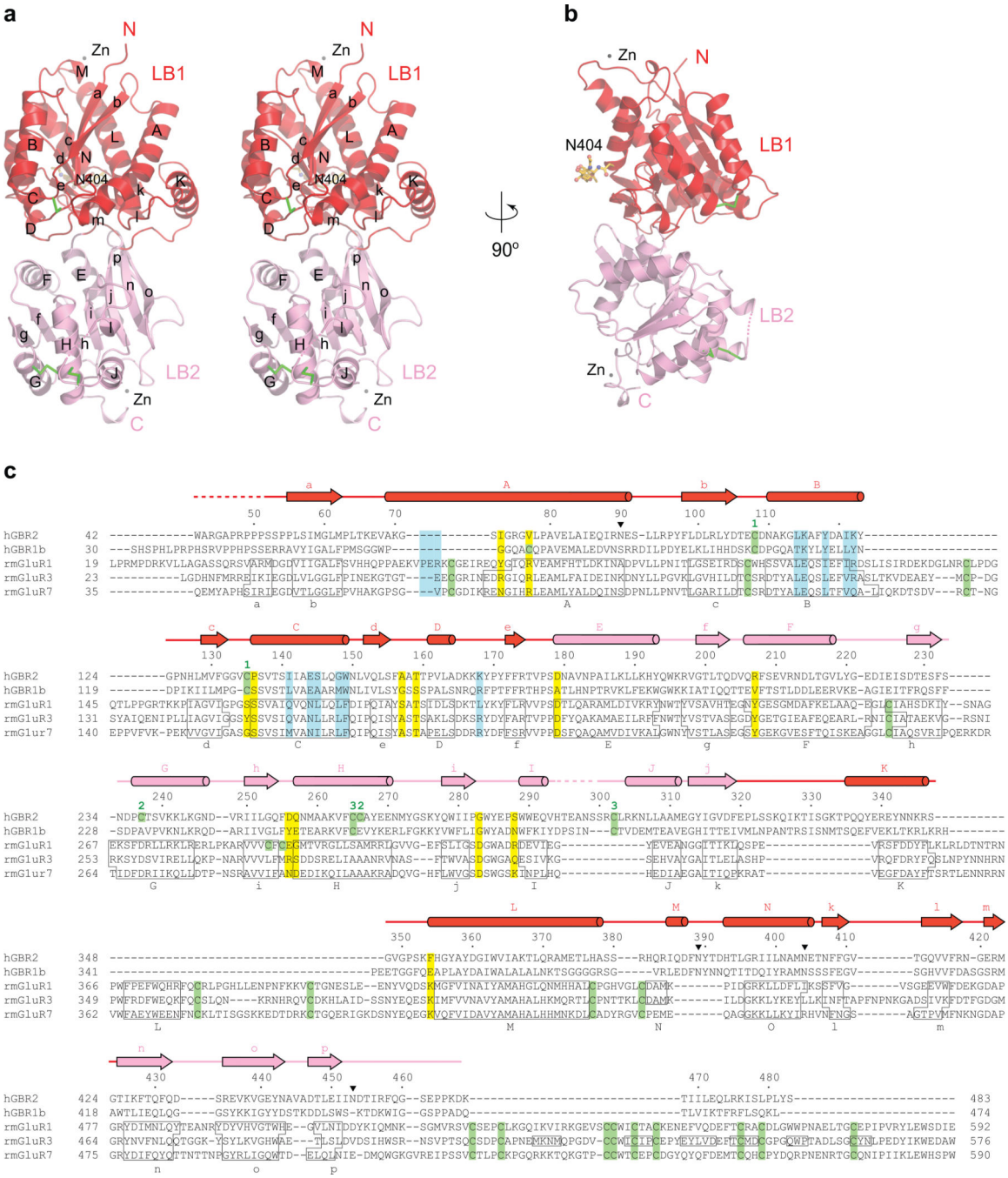

Figure 2. Crystal structure of human GBR2$_{VFT}$

(a) Stereo representation of the form I structure. LB1 and LB2 domains are colored red and pink, respectively. α-helices and β-strands are labeled using upper and lower case, respectively. Observed N-linked carbohydrates at N404 are in yellow. Disulfide bonds are in green. Two zinc ions are depicted as black spheres.

(b) 90° rotation of the GBR2$_{VFT}$ structure about the vertical axis.

(c) Structure-based sequence alignment of the extracellular regions of human GBR2, human GBR1b, and rat mGluR subtypes 1, 3, and 7. Secondary structure elements of GBR2$_{VFT}$ are

displayed above the alignment, labeled as in (a). α-helices are represented by cylinders, and β-strands by arrows. Disordered regions are marked by dotted lines. LB1 and LB2 domains are colored red and pink, respectively. Secondary structure assignments of mGluRs are boxed. Residues at the ligand-binding site of mGluR1 are colored yellow. Residues located at the dimer interfaces of both the free and complex forms of mGluR1 are highlighted in cyan. Cysteines are colored green; GBR2 disulfide bridges are indicated by pairs of numbers above the participating cysteines. GBR2 N-linked glycosylation sites are marked by black triangles.

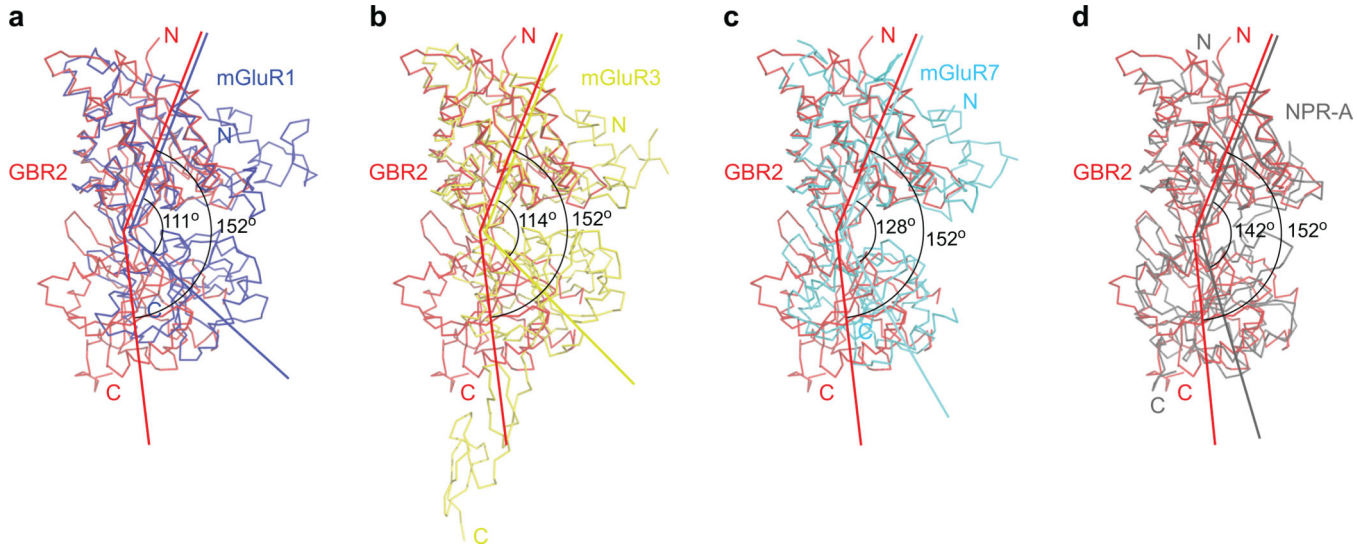

Figure 3.

Comparison of the interdomain hinge angles of human $GBR2_{VFT}$ (red) and (a) rat mGluR1 (blue), (b) rat mGluR3 (yellow), (c) rat mGluR7 (cyan), and (d) rat NPR-A (gray). Each structure was aligned with GBR2 based on the superposition of LB1 domains.

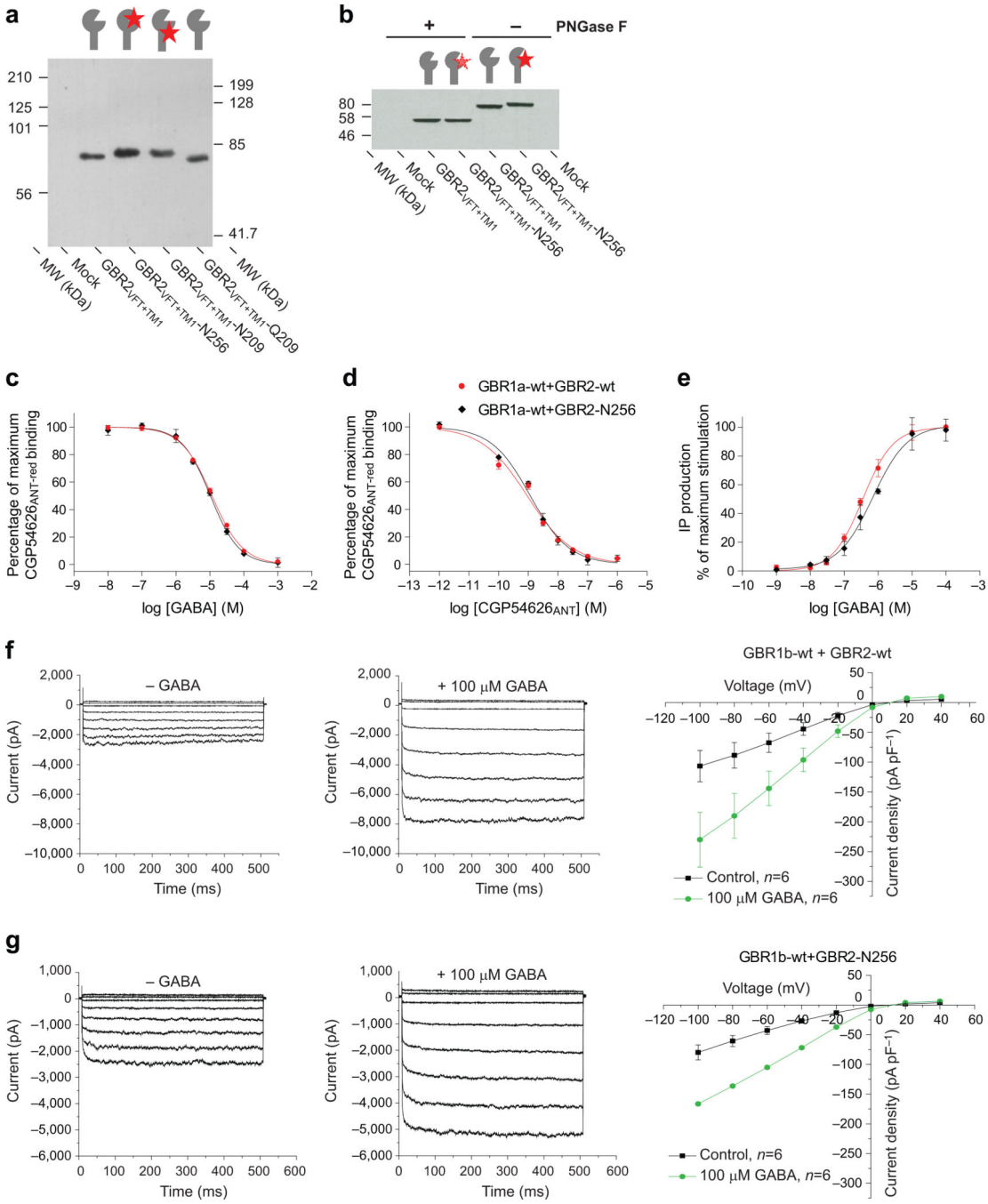

Figure 4. Analysis of N-glycosylated GBR2 mutants

(a) Western blot analysis of truncated GBR2 subunits lacking the TM and C-terminal regions. Lane 1 is membrane from mock transfected cells, and lanes 2, 3, 4 and 5 are membrane from cells transfected with wild-type $GBR2_{VFT+TM1}$, $GBR2_{VFT+TM1}$-N256, $GBR2_{VFT+TM1}$-N209, and $GBR2_{VFT+TM1}$-Q209, respectively.

(b) Western blot analysis showing the effect of PNGaseF treatment on wild-type $GBR2_{VFT+TM1}$ and $GBR2_{VFT+TM1}$-N256.

(c,d) Dose-response curves of (c) GABA and (d) $CGP54626_{ANT}$ inhibition of $CGP54626_{ANT}$-red binding on cells co-expressing GBR1a-wt with GBR2-wt (black) or with GBR2-N256 mutant (red).

(e) Dose-response curves of GABA-induced inositol phosphate (IP) production in cells co-expressing wild-type GBR1a (GBR1a-wt) with wild-type GBR2 (GBR2-wt, black) or with GBR2-N256 mutant (red).

(f,g) GABA-induced inwardly rectifying K^+ currents in cells co-expressing GIRK channel (GIRK1 & GIRK2) and (f) wild-type $GABA_B$ receptor (GBR1b-wt + GBR2-wt), or (g) the GBR2-N256 mutant (GBR1b-wt + GBR2-N256). The first two panels show the control recordings in the absence of GABA, and the currents induced by 100 μM GABA from a representative cell. The third panel shows the I-V relationship measured in the absence (black) and presence (green) of 100 μM GABA.

All data points represent mean ± s.e.m. of triplicate measurements or the indicated number (*n*) of experiments.

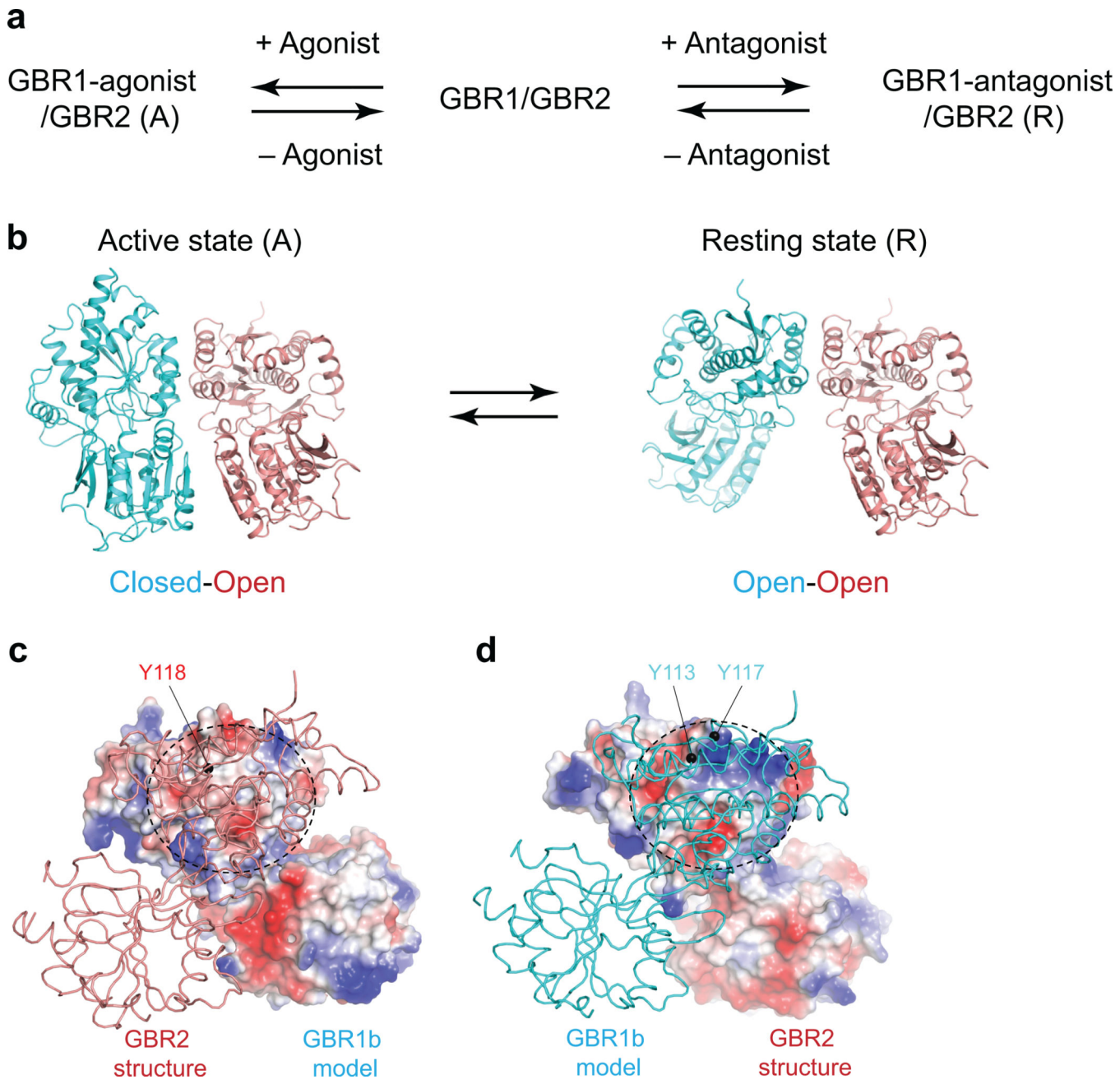

Figure 5. Heterodimerization interface of GBR2$_{VFT}$

(a) Dynamic equilibrium between free and ligand-bound GBR1$_{VFT}$-GBR2$_{VFT}$ heterodimer.

(b) Two structural models representing the active (closed-open/A) and resting (open-open/R) states of GBR1$_{VFT}$-GBR2$_{VFT}$ heterodimer. GBR1b$_{VFT}$ model is in cyan. GBR2$_{VFT}$ structure is in red.

(c) Electrostatic potential surface of the GBR1b$_{VFT}$ model showing the location of the potential dimerization interface (dotted circle). Structure of the bound GBR2$_{VFT}$ molecule is shown as a ribbon diagram in red. The view is a 90° rotation from that shown in (b). The location of Y118A in GBR2$_{VFT}$ is indicated by a black sphere.

(d) Electrostatic potential surface of $GBR2_{VFT}$ showing the location of the potential dimerization interface (dotted circle). The model for the bound $GBR1b_{VFT}$ molecule is drawn as a ribbon representation in cyan. The view is a 180° rotation from that shown in (c). The locations of Y113 and Y117 in $GBR1b_{VFT}$ are indicated by black spheres.

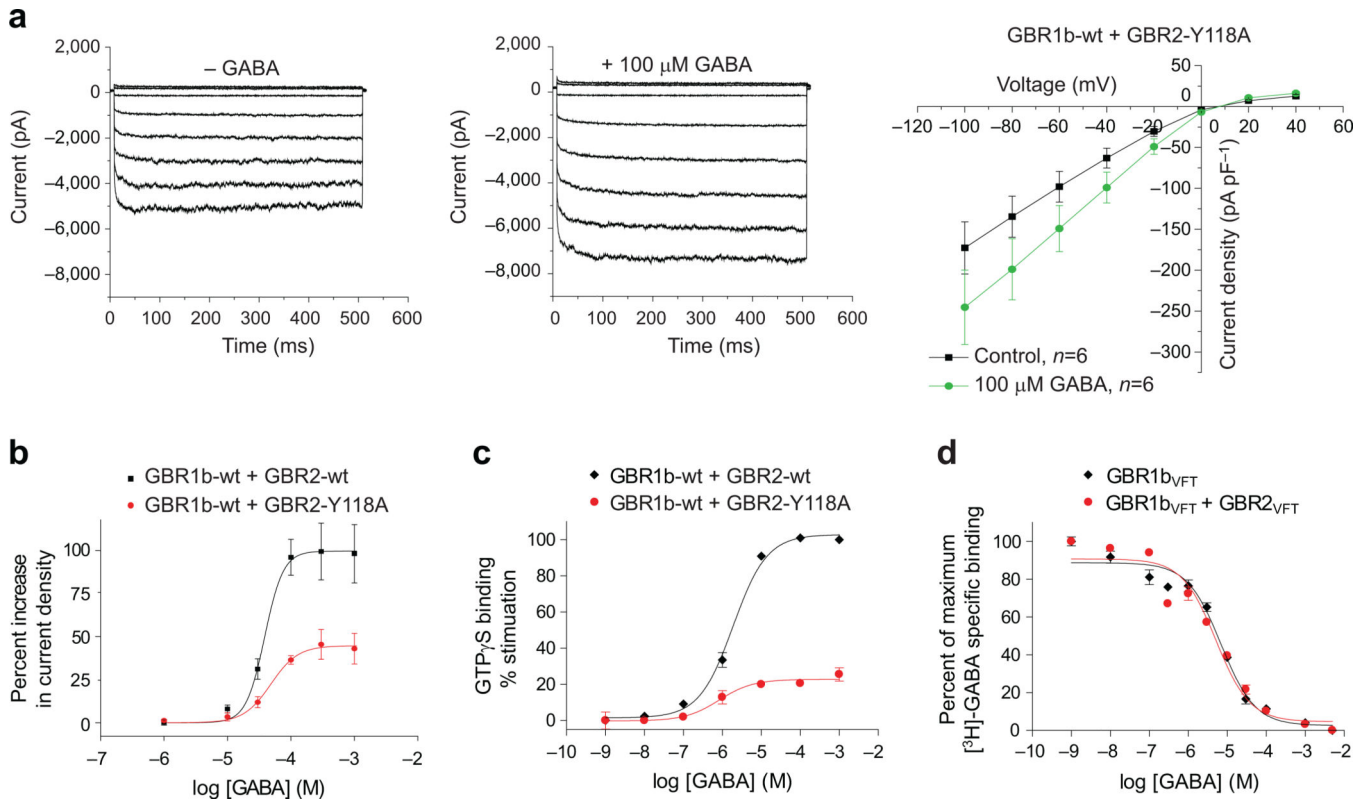

Figure 6. Effect of the GBR2 mutation Y118A on receptor function

(a) GABA-induced inwardly rectifying K^+ currents in cells co-expressing GIRK channel (GIRK1 & GIRK2) and the GBR2 mutant (GBR1b-wt + GBR2-Y118A). The first two panels show the control recordings in the absence of GABA, and the currents induced by 100 μM GABA from a representative cell. The third panel shows the I-V relationship measured in the absence (black) and presence (green) of 100 μM GABA.

(b) Dose-response analysis of percent increase in GIRK current density measured at −80 mV for wild-type $GABA_B$ receptor (GBR1b-wt + GBR2-wt, black), and GBR2 mutant (GBR1b-wt + GBR2-Y118A, red).

(c) GABA-stimulated dose-dependent [^{35}S]-GTPγS binding in membranes from cells expressing wild-type $GABA_B$ receptor (GBR1b-wt + GBR2-wt, black), or the GBR2 mutant (GBR1b-wt + GBR2-Y118A, red).

(d) Dose-response curves of the unlabeled agonist GABA inhibiting [^{3}H]-GABA binding to $GBR1b_{VFT}$ in the absence (black) or presence (red) of $GBR2_{VFT}$-Y118A.

All data points represent mean ± s.e.m. of triplicate measurements or the indicated number (*n*) of experiments.

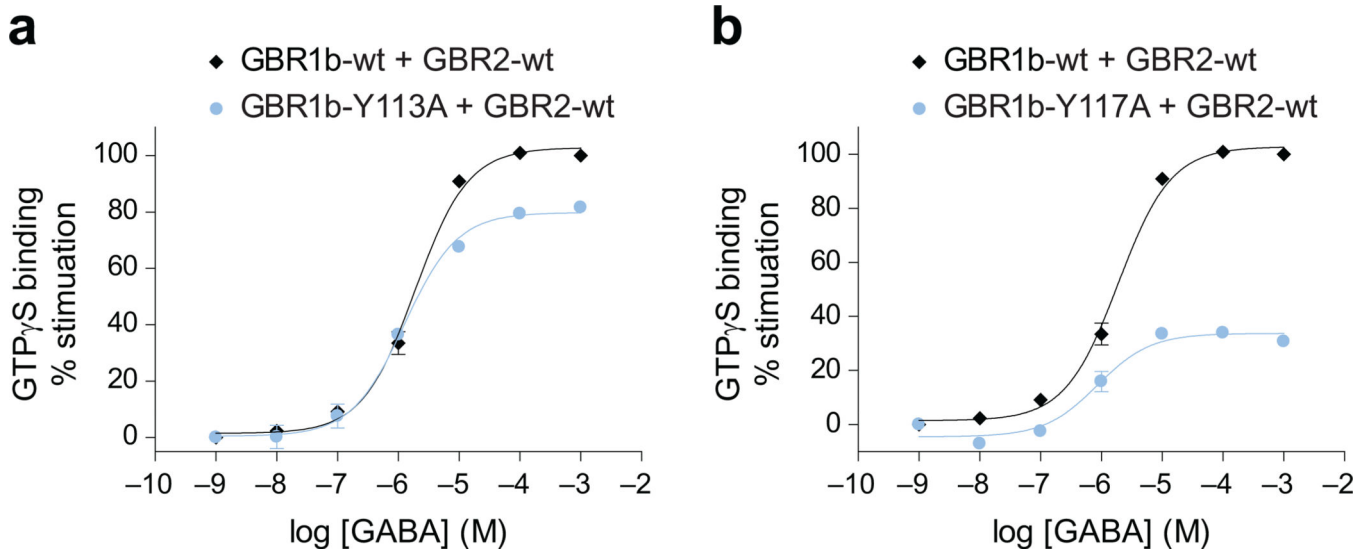

Figure 7. Effect of the GBR1b mutations Y113A and Y117A on receptor function

[^{35}S]-GTPγS binding in membranes from cells expressing GBR1b mutants (a) Y113A (GBR1b-Y113A + GBR2-wt) and (b) Y117A (GBR1b-Y117A + GBR2-wt). For each panel, GABA-stimulated dose-dependent [^{35}S]-GTPγS binding is shown in black for wild-type $GABA_B$ receptor (GBR1b-wt + GBR2-wt), and blue for the GBR1b mutant. Data points represent mean ± s.e.m. of triplicate measurements.

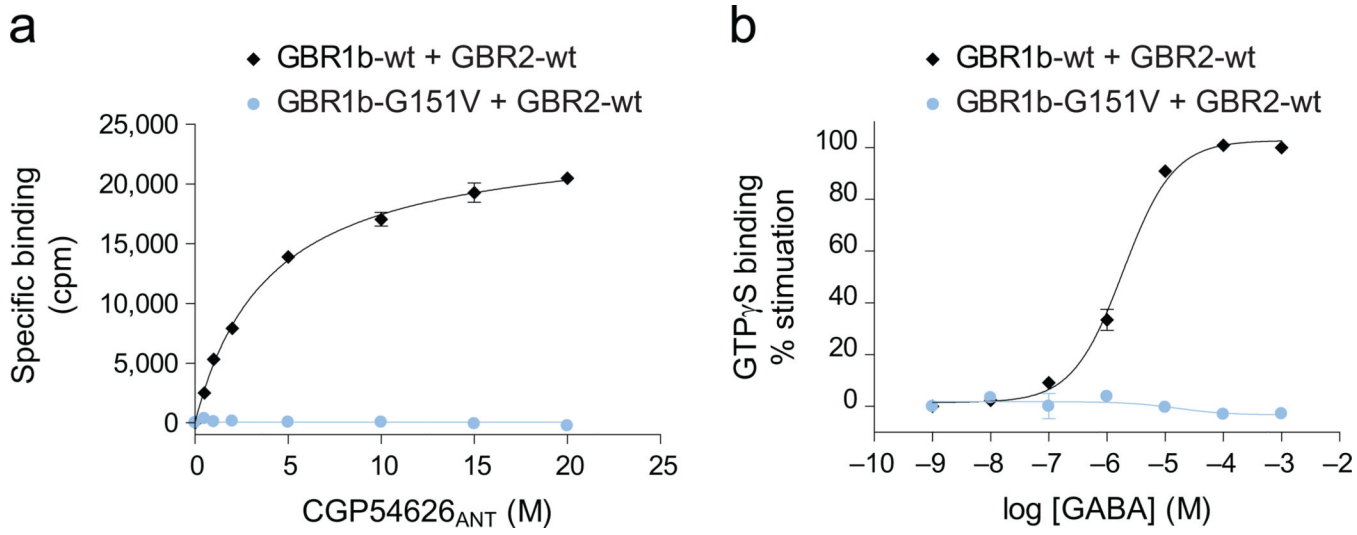

Figure 8. Effect of the GBR1b mutation G151 on ligand binding

(a) Dose-dependent [^{3}H]-CGP54626$_{ANT}$ binding, and (b) GABA-stimulated dose-dependent [^{35}S]-GTPγS binding in membranes from cells expressing the GBR1b-G151V mutant (GBR1b-G151V + GBR2-wt). Data is shown in black for wild-type GABA$_{B}$ receptor (GBR1b-wt + GBR2-wt), and blue for the GBR1b mutant. Data points represent mean ± s.e.m. of triplicate measurements.